Photoluminescence and radiationless processes in Mn^{2+}-doped $Ca_{1-x}Sr_xF_2$ fluorites as a function of pressure and temperature. A structural correlation study

F. Rodríguez[a] I. Hernández, and M. Moreno
DCITIMAC, Facultad de Ciencias, Universidad de Cantabria, Santander, Spain

R. Alcalá
Departamento de Física de la Materia Condensada, Universidad de Zaragoza, Spain

This work investigates the photoluminescence (PL) properties of Mn^{2+}-doped fluorites in CaF_2, BaF_2, SrF_2, and in solid solutions $Ca_{1-x}Sr_xF_2$. In particular, we focus on the radiationless processes leading to the surprising disappearance of the Mn^{2+} PL on passing from CaF_2: Mn^{2+} to SrF_2: Mn^{2+} or BaF_2: Mn^{2+}. For this purpose emission, excitation, lifetime, and time-resolved spectroscopy as a function of pressure and temperature are carried out in these compounds as well as in the $Ca_{1-x}Sr_xF_2$:Mn^{2+} ($x=0-1$) series using pressure spectroscopy. We show that the quenching of PL in these systems is associated with nonradiative thermal activated processes whose activation energy and pre-exponential rates strongly depend on the crystal volume irrespective of the chemical composition of the host crystal. A salient feature of this work deals with the increase of activation energy induced by pressure, whose variation with the lattice parameter is given by $E_a(\text{eV})=1.02-2.64\,(a\text{-}5.46)$, with $a(CaF_2)=5.46$ Å. It leads to a PL quantum yield enhancement, which favors appearance of Mn^{2+} PL even in the non-PL systems SrF_2:Mn^{2+} and BaF_2:Mn^{2+}. Furthermore, the activation energy mainly depends on the crystal volume per molecule irrespective of the crystal structure or the local symmetry around the impurity. In this way, the relevance of the fluorite-to-cotunnite phase transition to enhance PL is analyzed. This enhancement is explained in terms of the large volume reduction at the phase transition, as well as by the presence of low-symmetry crystal fields attained at the cation site yielding an increase of the radiative transition rate by the electric-dipole mechanism. © *2003 American Institute of Physics.*
[DOI: 10.1063/1.1611874]

I. INTRODUCTION

The photoluminescence (PL) properties of Mn^{2+}-doped MF_2 (M=Ca, Sr, Ba) fluorites have been matter of great interest because of their relevance as scintillators, phosphors and, in general, basic systems for the understanding of optical materials.[1-5] Particularly, these doped crystals are attractive since Mn^{2+} occupies the cation site of the fluorite structure with eightfold coordination, i.e., cubal complex MnF_8^{6-} (Refs. 1, 6–10) (see Fig. 1). This coordination provides a crystal-field (CF) at Mn^{2+} which is lower than that attained in sixfold octahedral coordination like Mn^{2+}-doped AMF_3 (A=Rb, K, Cs; M=Mg, Zn, Ca) fluoroperovskites.[11] The CF parameters, 10Dq, are about 0.5 and 1 eV for MnF_8^{6-} and MnF_6^{4-}, respectively, and, according to the Tanabe–Sugano diagram for d^5 ions,[12] are responsible for the green and red PL exhibited by Mn^{2+} in these systems.[1,13-16] Interestingly, the Mn^{2+} green-PL in the MnF_8^{6-} center is worthwhile for studying nonradiative processes in isolated impurities since multiphonon relaxation phenomena are *a priori* less probable than in MnF_6^{4-} red-PL systems, given that the number of phonons required to bridge the energy gap between the $^4T_{1g}$

excited state and the $^6A_{1g}$ ground state of Mn^{2+} in fluorites is almost twice that in fluoroperovskites. Besides, the $^4T_{1g} \rightarrow {}^6A_{1g}$PL placed at 2.53 eV (490 nm) in CaF_2: Mn^{2+}, decays with the longest lifetime ever measured among the transition metal ions ($\tau=182$ ms at 10 K) and its PL quantum yield is close to 1 ($\eta \approx 1$) at room temperature (RT) (Refs. 1 and 16). However, the Stokes shift for MnF_8^{6-} is by contrast significantly bigger than for MnF_6^{4-} thus favoring multiphonon-relaxation phenomena in fluorites with respect to perovskites.[15,17] The competition between energy gap and Stokes shift will finally determine conditions for radiationless phenomena.

In connection with this processes, PL changes unexpectedly along the fluorite series. Unlike CaF_2: Mn^{2+}, the isolated MnF_8^{6-} complex in isomorphous SrF_2: Mn^{2+} or BaF_2: Mn^{2+} is not PL either at RT or at any temperature at ambient pressure, respectively.[1,15,17] This surprising behavior is noteworthy for investigating nonradiative phenomena on the basis of structural correlations given that the local structure around Mn^{2+} is known from EPR and optical spectroscopy.[8,17]

The aim of this work is to understand the microscopic origin of the excited-state relaxation phenomena leading to radiationless process in Mn^{2+}-doped fluorites and how the

---

[a] Author to whom correspondence should be addressed. Electronic mail: rodriguf@unican.es
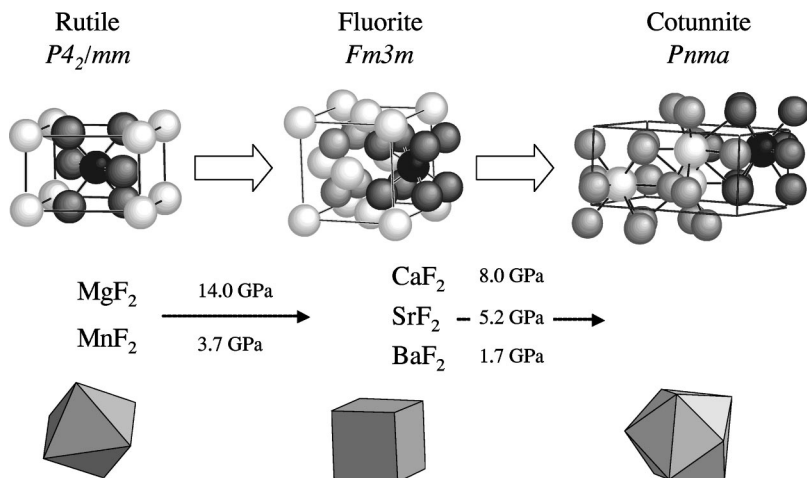
FIG. 1. Types of crystal structure of MF$_2$ (M: Mg, Mn, Ca, Sr, Ba) compounds, and coordination geometry around the cation in each phase. Values of the critical pressure in upstroke for the rutile-to-fluorite and fluorite-to-cotunnite are given in GPa. Structural transformations of the systems under study involve important changes of the cation site geometry. The local coordination at the cation site is shown at the bottom. It varies from sixfold coordination (rutile) to eightfold (fluorite) and ninefold noncentrosymmetric (cotunnite). Note that the critical pressure for the fluorite-to-cotunnite phase-transition decreases with the cation size (Refs. 28, 34–36).

host crystal affects it. This knowledge is crucial in order to control materials' PL.[7] For this purpose, we study the PL properties along the Ca$_{1-x}$Sr$_x$F$_2$: Mn^{2+} series by optical spectroscopy as a function of pressure and temperature. Attention is paid to the variation of the PL intensity, I_{PL}, and corresponding lifetime, τ, with temperature through the complete series of PL materials, and as a function of pressure in both PL and non-PL systems. This procedure has shown to be an excellent method to elucidate whether the loss of PL and the subsequent PL quenching on passing from CaF$_2$: Mn^{2+} to SrF$_2$: Mn^{2+} along the Ca$_{1-x}$Sr$_x$F$_2$: Mn^{2+} series is due to the different nature of the host cation (i.e., Ca^{2+} compared to Sr^{2+} or Ba^{2+}), or it is simply related to changes of lattice parameter with x, independent of the substituted cation.[1,15,18–20] Besides, it can reveal whether non-PL materials can be transformed into PL simply by reducing the volume of the host site. Previous pressure experiments for SrF$_2$: Mn^{2+} and BaF$_2$: Mn^{2+} demonstrate that the occurrence of PL is mainly related to the crystal volume.[21]

II. EXPERIMENT

Single crystals of MF$_2$ (M=Ca, Sr, Ba) and solid solutions Ca$_{0.5}$Sr$_{0.5}$F$_2$ and Ca$_{0.25}$Sr$_{0.75}$F$_2$ doped with MnF$_2$ (1.0% or 0.5% mol) were grown by the Bridgman technique as described elsewhere.[15,19] The presence of isolated Mn^{2+} ions at the cubal cation site (MnF$_8^{6-}$ complex) was checked by electron paramagnetic resonance (EPR) (Refs. 15 and 23).

PL spectra and lifetime measurements at room pressure were obtained using a ISA Fluoromax-2 fluorometer and a Chromex 500IS monochromator with a Tektronix 2430A oscilloscope, respectively. For lifetime measurements, the Mn^{2+} was excited with the 407 nm line of a Coherent I-302-K Krypton laser, which was modulated by a Newport 35085-3 acousto-optic modulator. Experiments in the 290–750 K range were done on a Leitz 350 heating stage. For low temperatures (10–350 K), we used a Scientific Instruments 202 closed-circuit cryostat and an APD-K controller. Hydrostatic pressure experiments were performed in a Diamond Anvil Cell (DAC; High Pressure Diamond Optics, Inc.). A mixture ethanol–methanol–water 16:3:1 was used as pressure transmitter, and the pressure was calibrated through the Ruby PL.[24] Single crystals of Mn^{2+}-doped fluorites (typical

dimensions: $100 \times 80 \times 40 \ \mu m^3$) were employed in pressure experiments. PL spectroscopy was accomplished by excitation into the $^4A_{1g}$, ^4E_g excited state of Mn^{2+} (O$_h$). Due to the extremely low PL quantum yield and lifetime of several crystals of the series $\eta \approx 0$; $\tau \approx 0$ for SrF$_2$:Mn^{2+} and BaF$_2$:Mn^{2+} at ambient conditions), we employed a high-sensitivity PL setup for measuring the PL lifetime and time-resolved spectroscopy under pressure.[21] Moreover, these Mn^{2+}-doped crystals exhibit a weak PL even for high quantum yields given that the MnF$_8^{6-}$ CF excitations ($^6A_{1g} \rightarrow {}^4\Gamma_i$) are spin and parity forbidden by the electric-dipole (ED) mechanism (oscillator strength $\sim 10^{-7}$) (Refs. 16 and 25) thus leading to very weak absorption peaks and long lifetime decays.

III. RESULTS AND DISCUSSION

A. Photoluminescence of the Ca$_{1-x}$Sr$_x$F$_2$: Mn^{2+} series at ambient conditions

Figure 2(a) depicts the excitation and corresponding emission (or PL) spectra for the luminescent materials of the Ca$_{1-x}$Sr$_x$F$_2$: Mn^{2+} series at ambient conditions. Excitation spectra have been normalized to the same intensity for comparison purposes. Note that the excitation spectra along the series are very similar and consist of four bands, which are characteristic of Mn^{2+} in a cubal coordination. Within this cubic symmetry, the band assignment of Fig. 2 is given in terms of electronic transitions from the $^6A_{1g}$ ground state to different excited spin-quartet states $^4\Gamma_i$. The values of the Racah parameters, B and C, and the CF parameter 10Dq obtained by fitting from the excitation spectra of the whole PL series are given in Table I. Note that the CF value, 10Dq=0.51 eV, is smaller than for Mn^{2+}-doped fluoroperovskites whose value varies from 10Dq=1.045 eV in KMgF$_3$: Mn^{2+} to 10Dq=0.854 in CsCaF$_3$: Mn^{2+} (Refs. 11, 13, and 14). The different CFs at the Mn^{2+} sites are associated with the longer local Mn–F distance in the fluorites (R_{Mn-F}=2.26 Å for CaF$_2$: Mn^{2+}) (Refs. 8 and 17) than in the fluoroperovskites (R_{Mn-F}=2.07 Å for KMgF$_3$: Mn^{2+} and R_{Mn-F}=2.15 Å for CsCaF$_3$: Mn^{2+}) (Refs. 11, 13, and 14). The 10Dq reduction by a factor two on passing from CaF$_2$: Mn^{2+} to KMgF$_3$: Mn^{2+} is consistent with a

TABLE I. Emission and excitation energies, together with the associated Stokes shift, measured by optical spectroscopy along the $Ca_{1-x}Sr_xF_2$: Mn^{2+} series for $x=0$, 0.25, 0.50, and 0.75 at $T=290$ K. The calculated excitation energies are given in parenthesis, together with corresponding Racah parameters, B and C, and the crystal-field, 10Dq, parameter. The C/B ratio was obtained from the two 10Dq-independent $^4A_{1g}$, ^4E_g (G), and ^4E_g(D) energies, while B and 10Dq derived by fitting using all transition energies. The Trees and Seniority parameters for Mn^{2+} were kept fixed: $\alpha=8.3$ meV (67 cm^{-1}) and $Q=-16.2$ meV (-131 cm^{-1}) (Ref. 13). The fluorite lattice parameter of each crystal determined from x-ray diffraction is also included (Ref. 15).

x	a (Å)	Emission (eV)	$^4T_{1g}(^4G)$	$^4T_{2g}(^4G)$	$^4A_{1g}$, $^4E_g(^4G)$ (eV)	$^4T_{2g}(^4D)$	$^4E_g(^4D)$	$^4T_{1g}(^4P)$	B (cm^{-1})	C (cm^{-1})	10Dq (cm^{-1})	Stokes shift (eV)/(cm^{-1})
0	5.46	2.53	2.80	3.09	3.14	3.69		3.91	0.094	0.411	0.514	0.27
			(2.83)	(3.09)	(3.16)	(3.61)	(3.70)	(3.82)	760	3310	4150	2200
0.25	5.56	2.48	2.83	3.10	3.15	3.69		3.90	0.095	0.413	0.524	0.35
			(2.84)	(3.11)	(3.18)	(3.63)	(3.73)	(3.85)	765	3335	4225	2800
0.50	5.64	2.47	2.84	3.10	3.15	3.70		3.90	0.095	0.413	0.506	0.37
			(2.86)	(3.11)	(3.18)	(3.64)	(3.73)	(3.83)	765	3335	4080	3000
0.75	5.74	2.49	2.87	3.11	3.15	3.71		3.90	0.095	0.413	0.468	0.38
			(2.89)	(3.12)	(3.18)	(3.65)	(3.73)	(3.81)	765	3335	3775	3100

R_{Mn-F}-dependence of 10Dq on the basis of $10Dq=KR_{Mn-F}^{-5}$ and considering that $10Dq(Cubal)=8/9 \, 10Dq(Octahedral)$ (Refs. 19, 26, and 27). So that

$$\frac{10Dq(CaF_2:Mn^{2+})}{10Dq(KMgF_3:Mn^{2+})} = \frac{0.51}{1.045} = 0.49$$

$$\approx \frac{8}{9}\left(\frac{R_{Mn-F}(KMgF_3)}{R_{Mn-F}(CaF_2)}\right)^5 = \frac{8}{9}\left(\frac{2.07}{2.26}\right)^5$$

$$= 0.57.$$

The compound series exhibits a unique PL band, which is associated with the same MnF_8^{6-} formed complex. This band occurs at 2.53 eV (490 nm green-PL) in contrast to the red-PL of MnF_6^{4-} in the fluoroperovskites (1.45 eV) and is a consequence of the smaller CF in the fluorites (Table I). The fit 10Dq parameter and its variation along the series (Table I) follow the variation of R_{Mn-F} given elsewhere.[27]

Aside from this, the Mn^{2+} PL in fluorites is noteworthy. Although the excitation spectra of Fig. 2 and Table I imply that the local structures of Mn^{2+} are similar along the series, the PL intensities and lifetimes show a surprising behavior [Fig. 2(b)]. While the PL is similar for $x=0$, 0.25, and 0.5 at

ambient conditions, both I_{PL} and τ decrease by a factor four for $x=0.75$ and disappear ($I_{PL}\approx0$ and $\tau\approx0$) for SrF$_2$: Mn^{2+} and of course for BaF$_2$: Mn^{2+} (Refs. 15, 17, and 21). τ decreases with the strontium fraction from 56 to 16 ms on passing from $x=0.5$ to $x=0.75$, and the general behavior of $\tau(x)$ shows a close correlation with $I_{PL}(x)$. Nevertheless, such a correlation between I_{PL} an τ is not shown by the Stokes shift (Table I), whose value increases along the series: Abruptly from $x=0$ to $x=0.25$ and slightly from $x=0.25$ to 1. An adequate description of the PL behavior requires temperature-dependence studies, and especially when, as we show later, the nonradiative PL-quenching process is thermally activated.

B. Variation with temperature

1. Photoluminescence and lifetime in CaF$_2$: Mn^{2+}

Figure 3 shows PL lifetime measurements for CaF$_2$: Mn^{2+} at temperatures from 10 to 750 K. This figure shows that the PL strongly depends on the temperature and thermal quenching takes place above 600 K. The analysis of $\tau(T)$ indicates that there are several distinguishable contributions to the thermal evolution of the $^6A_{1g}\rightarrow{^4T_{1g}}$ de-excitation
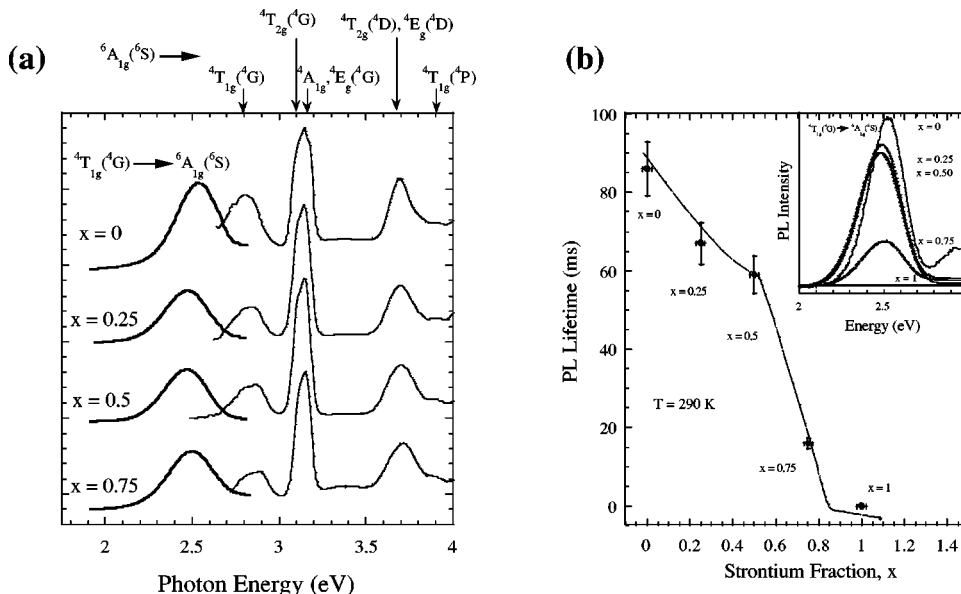

FIG. 2. (a) Variation of the emission (photoluminescence) (thick line) and excitation (thin line) spectra along the $Ca_{1-x}Sr_xF_2$: Mn^{2+} series ($x=0$, 0.25, 0.50, 0.75, and 1) at room temperature. Bands are assigned to crystal field transition within the Mn^{2+} cubal coordination (O_h symmetry) according to the Tanabe–Sugano diagram for d^5 ions (Table I). (b)Variation of photoluminescence lifetime $\tau(x)$ along the $Ca_{1-x}Sr_xF_2$: Mn^{2+} series. The photoluminescence time dependence follows a single exponential behavior and the lifetime was obtained by fitting the decay curve $I_{PL}(t)$ to the expression $I_{PL}(t)=I_{PL}(0)\,e^{-t/\tau}$. The inset shows the variation of the emission spectrum along the series under the same excitation conditions. The integrated intensity obtained from the PL spectra follows the same behavior with x than the lifetime $\tau(x)$.

J. Chem. Phys., Vol. 119, No. 16, 22 October 2003

Fluorescence in Mn^{2+}-doped Ca$_{1-x}$Sr$_x$F$_2$ 8689

process and $\tau^{-1}(T)$. These can be described by two radiative and one nonradiative term through the equation:[1,20]

$$\tau^{-1} = \tau_{rad}^{-1}(T) + \tau_{non\text{-}rad}^{-1}(T)$$

$$= \tau_0^{-1} + \tau_{ED}^{-1}\text{Coth}\frac{\hbar\omega_u}{2kT} + w_{NR}(T). \qquad (1)$$

The two radiative terms represent (1) the temperature-independent transition rate, including contributions from the magnetic-dipole (MD) as well as ED components due to noncentrosymmetric static distortions, and (2) the ED vibration-assisted mechanism, where τ_{ED}^{-1} is the ED rate from zero-point vibrations and ω_u is the vibrational frequency. This term enables PL de-excitation through the ED mechanism in isolated centrosymmetric transition–metal complexes.[27] The third nonradiative term contains the rate for radiationless processes.[1,15,20] In the present systems, the nonradiative rates are well described by an Arrhenius-type law $w_{NR} = p \exp(-E_a/kT)$, where E_a is the activation energy and p is the associated rate. Equation (1) implies that all these systems experience radiationless de-excitation upon increasing temperature. $I_{PL}(T)$ is related to this mechanism through $\tau_{rad}^{-1}(T)$ and the PL quantum-yield, η, as

$$I_{PL}(T) \propto \tau_{rad}^{-1}\eta = \tau_{rad}^{-1}\frac{\tau_{rad}^{-1}}{\tau_{rad}^{-1} + p \cdot e^{-E_a/kT}}, \qquad (2)$$

where τ_{rad}^{-1} is proportional to the integrated band intensity of the $^6A_{1g} \rightarrow {}^4T_{1g}$ band in the optical absorption spectrum.

The long lifetime measured at low temperature, $\tau(10\,K) = 186$ ms,[1,15,20] is consistent with the doubly spin and parity forbiddances of the $^6A_{1g} \leftrightarrow {}^4T_{1g}$ transition and characteristic of isolated Mn^{2+} impurities.[16,25–27]

Similar thermal behaviors of the PL are also observed for the Ca$_{1-x}$Sr$_x$F$_2$: Mn^{2+} series, although the parameters involved in Eq. (2) vary with x, i.e., the strontium content.

2. Photoluminescence quenching along the fluorite Ca$_{1-x}$Sr$_x$F$_2$: Mn^{2+} series

The PL along the series can be accounted for on the basis of findings in CaF$_2$: Mn^{2+}. Figure 4(a) depicts the $I_{PL}(T)$ curves and the corresponding $\tau^{-1}(T)$ curves in a wide temperature range around the quenching temperature. PL quenching occurs at a different temperature for each crystal, as found previously.[15] Nevertheless, in this work, we report precise measurements of $I_{PL}(T)$ and $\tau(T)$ around the PL quenching and interpret them in terms of Eqs. (1) and (2). We have previously shown[19,20] that the decrease of $I_{PL}(T)$ follows Eq. (2). In fact, the $\ln[[I_{PL}^{max}/I_{PL}(T)]-1]$ is linear with $1/T$ thus providing the values of E_a directly. The so determined values are given in Table II and Fig. 5(a). The proposed de-excitation mechanism is also confirmed by the variation of $\tau^{-1}(T)$, whose experimental data and corresponding fits to Eq. (1) are given in Fig. 4(b). In contrast to $I_{PL}(T)$, $\tau^{-1}(T)$ not only provides the activation energy involved in the nonradiative process but also on the de-excitation rate, p. We obtain similar E_a values either from $I_{PL}(T)$ or $\tau^{-1}(T)$, thus providing model consistency (Table II). From the data analysis we conclude that E_a varies linearly with the strontium content along the series as $E_a(x)$
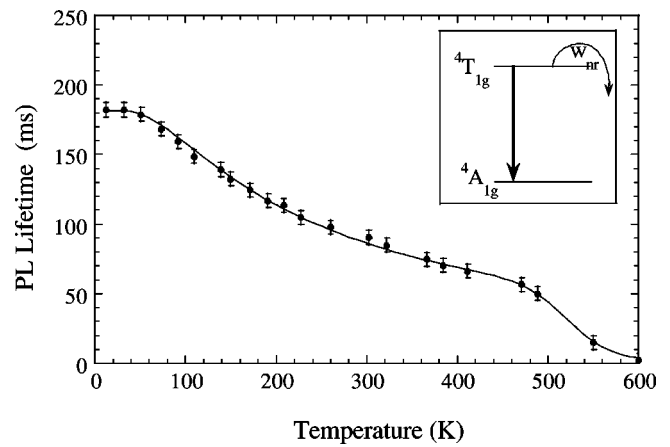

FIG. 3. Variation of the PL lifetime with temperature, $\tau(T)$, in CaF$_2$: Mn^{2+}. The solid line represents the least-square fit to Eq. (1). The figure illustrates the three different contributions to the variation of $\tau(T)$ in terms of their associated transition rates: $\tau^{-1}(T) = \tau_{rad}^{-1}(T) + \tau_{non\text{-}rad}^{-1}(T)$, where the radiative rate is given by $\tau_{rad}^{-1}(T) = \tau_0^{-1} + \tau_{ED}^{-1}\text{Coth}(\hbar\omega_u/2kT)$ while the nonradiative rate is $\tau_{non\text{-}rad}^{-1}(T) = w_{NR}(T) = p \cdot \exp(-E_a/kT)$. The fit parameters are: $\tau_0^{-1} = 2.2$ s^{-1}, $\tau_{ED}^{-1} = 3.3$ s^{-1}, $\hbar\omega_u = 20$ meV, $p = 8.4 \times 10^{10}$ s^{-1}, and $E_a = 1.010$ eV.

$= 1.017 - 0.930\,x$. Or analogously, E_a is linearly related to the lattice parameter, a, taking into account the linear dependence of a and x as $a(x) = 0.35\,x + 5.46$ (Ref. 15) So that $E_a(a) = 1.017 - 2.641[a - 5.46]$ (in eV and Å units for E_a and a, respectively). A salient feature of the present work is the strong dependence of the pre-exponential factor, p, with either x or a. This parameter varies exponentially along the series according to Fig. 5(b) as: $p(x) = 6.5 \cdot 10^9 \exp(-9.9x)$, or $p(a) = 6.5 \cdot 10^9 \exp[-28.1(a - 5.46)]$. These results indicate that PL properties and quenching along the fluorite series can be explained on the basis of Eq. (1) with parameters E_a and p depending on either x or a.

The question arising at this stage is whether the variation of E_a along the series is due to the different chemical nature of the host cation either Ca^{2+} or Sr^{2+} (or Ba^{2+}) or it is directly related to the host crystal size, i.e., the lattice parameter. To determine which, we performed pressure experiments for selected compounds of the series.

TABLE II. Fit parameters $E_a(x)$ and $p(x)$ derived from variations of the PL intensity with temperature through the $\text{Ln}[[I_{PL}^{MAX}/I_{PL}(T)]-1]$ vs $1/T$ plot (Refs. 19 and 20) and from variations of the lifetime with temperature through the $\tau^{-1}(T)$ vs T plot in Ca$_{1-x}$Sr$_x$F$_2$: Mn^{2+} for $x = 0$, 0.25, 0.5, and 0.75 [Fig. 4(b)].

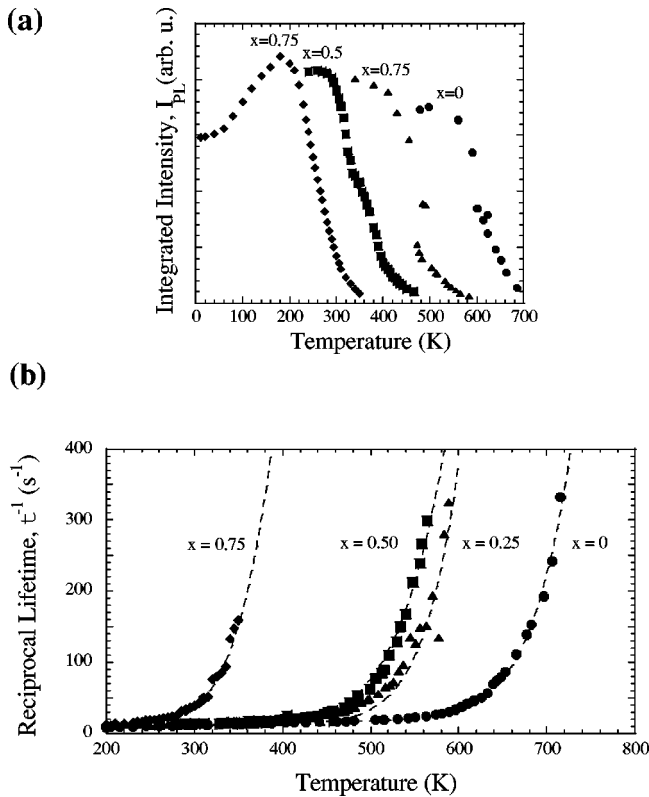| Strontium content x	PL intensity Activation energy E_a (eV)	PL lifetime	
		Pre-exponential factor p (s^{-1})	Activation energy E_a (eV)
0	1.08(10)	$4\,(2) \times 10^9$	1.01 (10)
0.25	0.69(10)	$1.4\,(7) \times 10^9$	.83 (10)
0.5	0.40(10)	$2.1(1.0) \times 10^7$	0.69 (10)
0.75	0.30(10)	$4\,(2) \times 10^6$	0.34 (10)

(a)

(b)

FIG. 4. (a) Variation of the integrated PL intensity with the temperature, $I_{PL}(T)$, along the $Ca_{1-x}Sr_xF_2$: Mn^{2+} series. Note that the PL quenching takes place upon heating at a different temperature for each compound. The higher the strontium content x, the lower the quenching temperature. The decay of $I_{PL}(T)$ of each compound follows an Arrhenius-type behavior, characteristic of nonradiative de-excitation processes. The analysis of the $I_{PL}(T)$ quenching (Refs. 19 and 20) provides the activation energies, E_a [see text and Fig. 5(a)]. (b) Variation of the reciprocal lifetime with temperature, $\tau^{-1}(T)$, in the $Ca_{1-x}Sr_xF_2$: Mn^{2+} series. Lines represent fits of the experimental data to Eq. (1). The variations are consistent with the de-excitation rates described by Eq. (1), and $I_{PL}(T)$ data of (a). The fits of $\tau^{-1}(T)$ to Eq. (1) provide the activation energies, $E_a(x)$, but also the pre-exponential factors, $p(x)$, involved in the Arrhenius law governing the radiationless process. Table II collects the parameters $E_a(x)$ and $p(x)$.

C. Pressure spectroscopy in Mn^{2+}-doped $Ca_{1-x}Sr_xF_2$. Structural correlations

1. Highly efficient materials

Figure 6 reports the pressure experiments on the most efficient of these PL materials. The PL lifetime is the appropriate parameter for the present study since it can be directly related to the microscopic model through Eq. (1).

Figures 6 and 7 show the variation of the PL spectra and corresponding lifetimes as a function of pressure in CaF_2: Mn^{2+} and $Ca_{0.5}Sr_{0.5}F_2$: Mn^{2+}. These systems are interesting since $\eta \approx 1$ at ambient conditions, i.e., $w_{NR} \approx 0$, according to their respective p and E_a values and Eq. (2). The PL spectrum of CaF_2: Mn^{2+} does not vary significantly with pressure. As Fig. 6(b) shows, the transition energy slightly shifts to lower energy from 2.53 eV at ambient conditions to 2.52 eV at 4.3 GPa. However, $\tau(P)$ increases from 86 ms at ambient pressure to 96 ms at 5 GPa. The increase of $\hbar\omega_u$ with P cannot explain the observed variation in terms only of the $Coth(\hbar\omega_u/2kT)$ factor. This term is estimated to account for not more than 50% of such variation if we assume that the
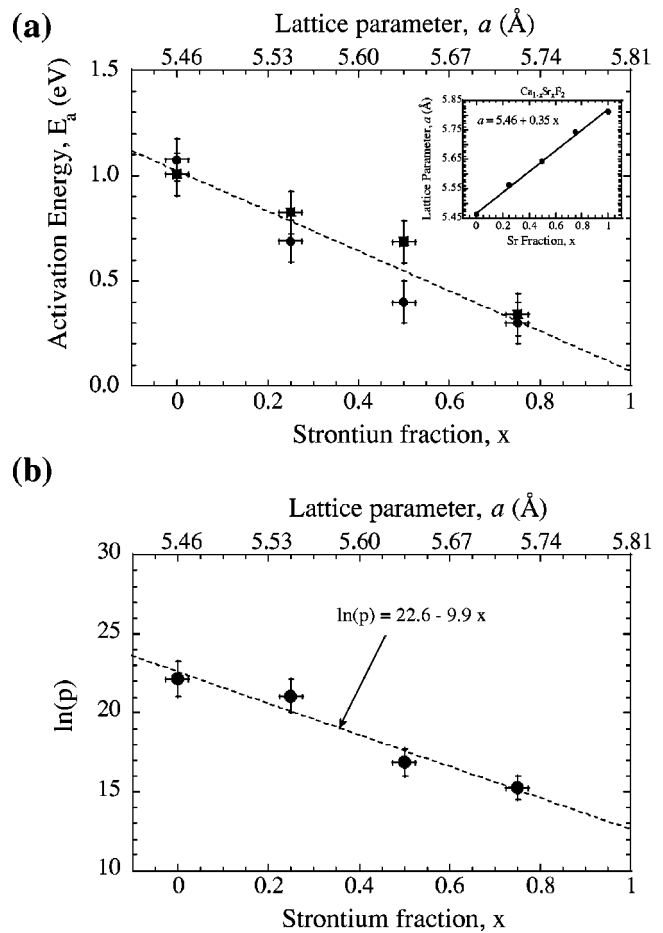
(a)

(b)

FIG. 5. Variation of the (a) activation energy, $E_a(x)$, and (b) logarithm of the preexponential factor, Ln $p(x)$, with the strontium fraction, x, along the $Ca_{1-x}Sr_xF_2$: Mn^{2+} series. An analogous variation as a function of the lattice parameter, $E_a(a)$ and Ln $p(a)$. The transformation takes into account the linear relation between a and x through the expression given in the inset (Ref. 15). Squares and circles represent data from $I_{PL}(T)$ and $\tau^{-1}(T)$, respectively (see text). The straight dotted lines correspond to linear least-square fits. The activation energy E_a is found to follow equation $E_a = 1.02 - 0.93\,x$, i.e., $E_a = 1.02 - 2.64\,(a - 5.46)$ and the pre-exponential factor: $p(x) = 6.5\ 10^9 e^{-9.9\,x}$ or, equivalently, $p(a) = 6.5\ 10^9 e^{-28.1\,(a-5.46)}$.

Grüneisen parameter associated with the enabling mode is similar to $\gamma = 1.34$ corresponding to the Raman a_{1g} mode for CaF_2 (Ref. 28). This assumption likely provides an overestimation of the pressure-variation of $\hbar\omega_u$ since, in general, γ for stretching modes is usually greater than for bending modes.[29] Actually, the observed increase of $\tau(P)$ can be explained taking into account an additional contribution associated with an enhancement of the vibration-assisted ED transition rate, τ_{ED}^{-1}, by the reduction of R_{Mn-F} with P.[20] In fact, a shortening of the Mn–F distance will increase the F^--to-Mn^{2+} charge-transfer (CT) energy leading to a reduction of the $^4T_{1g}$ PL state mixing with odd-parity CT states, which are responsible for the ED enabling mechanism through vibrational assistance.

The experimental $\tau^{-1}(P)$ data can be accounted for by including a pressure-dependent rate $\tau_{ED}^{-1}(P) = \tau_{ED}^{-1}(0) - \alpha\,P$ in Eq. (1) where α is a positive value and the minus sign is related to the pressure induced reduction of the transition probability. The $\tau(P)$ curve shown in Fig. 6(b) for CaF_2:
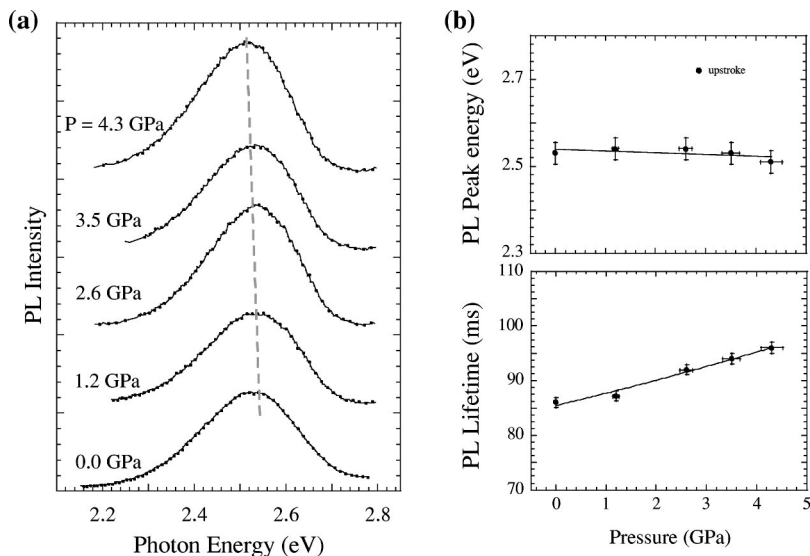
FIG. 6. (a) Variation of the PL spectrum with pressure for CaF$_2$: Mn^{2+} at room temperature. The straight line is a guide for the eye. (b) Variation of the PL energy with pressure (top) and corresponding lifetime with pressure (bottom). The solid line represents the fit of experimental data to the expression $\tau^{-1}(P) = \tau_0^{-1} + (\tau_{ED}^{-1}(0) - \alpha P)\mathrm{Coth}[\hbar\omega_u(P)/2kT]$. The fit parameters are $\tau_0^{-1} = 2.6\ \mathrm{s}^{-1}$, $\tau_{ED}^{-1}(0) = 3.5\ \mathrm{s}^{-1}$, $\alpha = 0.16\ \mathrm{s}^{-1}\ \mathrm{GPa}^{-1}$ and $\hbar\omega_u(P) = 20 + 0.45\ P$ (units in meV and GPa, respectively). In this system the nonradiative transition rate is $w_{NR} \approx 0$ in the whole pressure range (see text).

Mn^{2+} was fit to Eq. (1) with $\alpha = 0.16\ \mathrm{s}^{-1}\ \mathrm{GPa}^{-1}$. This value is consistent with the proposed model taking into account the variation of the CT states with the local distance as obtained from MS–Xα calculations performed on the MnF$_6^{4-}$ complex.[30–32]

A pressure-induced enhancement of $\tau(P)$ takes place also in the compound Ca$_{0.5}$Sr$_{0.5}$F$_2$: Mn^{2+}. Nevertheless, the main feature of the variation of $\tau(P)$ in this system is the fluorite-to-cotunnite structural phase-transition (Fig. 1). Apart from Raman, phase-transition is evidenced by PL through the abrupt variation of both τ (from 56 to 13 ms) and the abrupt redshift of 0.11 eV at $P = 5.2$ GPa in upstroke. A similar but opposite variation is observed at 2.2 GPa in downstroke, thus indicating a pressure hysteresis of 3.0 GPa. Interestingly, the lifetime decrease in the cotunnite phase is not associated with an increase of radiationless phenomena given that I_{PL} does increase with pressure along with this phase. The loss of inversion center in the ninefold coordinated MnF$_9^{7-}$ in the cotunnite phase can explain this feature. Therefore, we associate the decrease of $\tau(P)$ at phase-transition with the presence of noncentrosymmetric CF at the Ca^{2+} or Sr^{2+} sites in the cotunnite phase, which enables the ED mechanism.

2. Low efficiency materials: Pressure-induced photoluminescence

Figure 8(a) shows the variation $\tau(P)$ in the weakest PL crystal of the series: Ca$_{0.25}$Sr$_{0.75}$F$_2$: Mn^{2+}. A remarkable feature is the surprising PL enhancement experienced by this crystal upon pressure. $\tau(P)$ changes from 16 to 50 ms in the range 0–4 GPa range, reaching the PL properties attained in Ca$_{0.5}$Sr$_{0.5}$F$_2$: Mn^{2+} at ambient conditions. The behavior of $\tau(P)$ in this pressure range can be accounted for on the basis of Eq. (1) by replacing $E_a(P)$ by the corresponding $E_a(a)$ through the Murnaghan equation of state (EOS):[29]

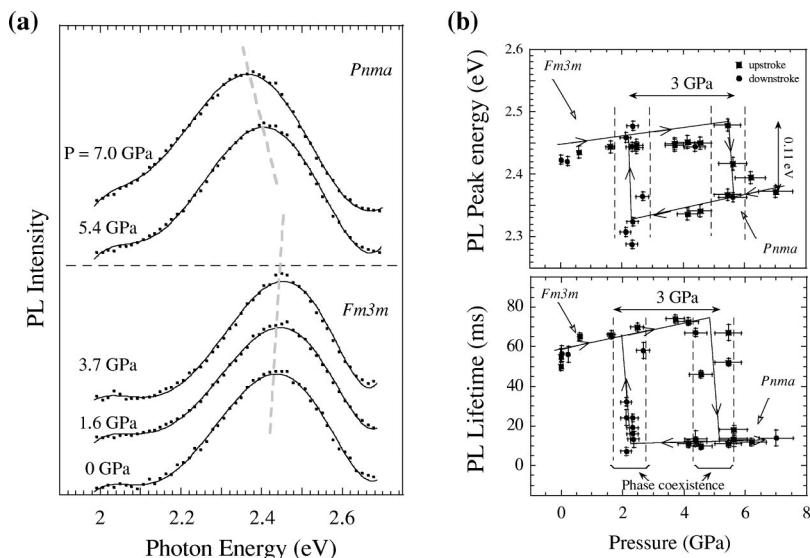$$V = V_0\left(1 + \frac{B'}{B_0}P\right)^{-1/B'}. \tag{3}$$

FIG. 7. (a) Variation of the PL spectrum with pressure for Ca$_{0.5}$Sr$_{0.5}$F$_2$: Mn^{2+} at room temperature. (b) Evolution of the PL energy (top) and corresponding lifetime (bottom) with pressure. The abrupt jump of $E(P)$ and $\tau(P)$ observed at $P = 5$ GPa in upstroke corresponds to the occurrence of the fluorite-to-cotunnite phase-transition. The reverse behavior is observed at $P = 2$ GPa in downstroke thus indicating a phase-transition hysteresis of $\Delta P = 3$ GPa. Lines are guides for the eye and show the pressure runs.

The line of Fig. 8(b) has been obtained from that EOS using $V_0 = 5.46$ Å^3, $B_0 = 73.4$ GPa, and $B' = 5$ (Refs. 22, 28, and 33). The fair agreement between calculated and experimental $\tau(P)$ confirms the volume dependence of E_a irrespective of the composition of the host crystal. Therefore, we conclude that the variation of Mn^{2+} PL along the series must be ascribed to the change of volume provided by replacing Ca^{2+} for Sr^{2+}.

$\tau(P)$ decreases from 60 to 14 ms just above 4 GPa. However, this decrease is not accompanied by a loss of PL; indeed $I_{PL}(P)$ increases above 4 GPa. Aside $I_{PL}(P)$ and $\tau(P)$, the PL change is also evidenced by an abrupt redshift of the PL band by -0.16 eV as it is shown in Fig. 8(b). Analogously to findings in Ca$_{0.5}$Sr$_{0.5}$F$_2$: Mn^{2+}, this PL behavior is associated with the fluorite-to-cotunnite phase-transition at 4.0 GPa in upstroke for the present system.

The relevance of the cotunnite phase to enhance PL properties in the title materials was previously pointed out.[21] The occurrence of this high-pressure phase is responsible for the appearance of Mn^{2+} PL above $P = 7.5$ GPa in BaF$_2$: Mn^{2+} which is not PL at ambient pressure.[21] If this phase-transition did not occur the critical pressure required to induce Mn^{2+} PL within the fluorite phase of BaF$_2$ is estimated to be $P = 30$ GPa according to Eq. (1) and the structural correlations established in Fig. 5(b) and Table I. As we will see later, this pressure in BaF$_2$ roughly corresponds to a critical lattice parameter, $a_c = 5.75$ Å, i.e., a relative volume reduction of $\Delta V/V = -22\%$. In conclusion, Mn^{2+} PL in the fluorite phase in BaF$_2$: Mn^{2+} is possible whenever the host crystal fulfills the condition $a < a_c$. Accordingly, the main reason for pressure-induced PL in the cotunnite phase in BaF$_2$: Mn^{2+} at moderate pressure is the important volume reduction of 10% attained at the first-order phase-transition at $P = 1.7$ GPa (Fig. 1).

Interestingly, the non-PL SrF$_2$: Mn^{2+} at ambient pressure becomes PL in the fluorite phase above $P = 3.8$ GPa in upstroke.[21] Above this pressure the condition $a(P) < a_c$ for the occurrence of the Mn^{2+} PL truly holds. Like BaF$_2$: Mn^{2+}, PL enhances upon phase-transition to the cotunnite phase at $P = 4.0$ GPa. Interestingly, Mn^{2+} PL persists in the high-pressure cotunnite phase in downstroke due to the high phase-transition hysteresis. However, PL disappears below the phase-transition pressure in the recovered fluorite phase at $P = 1.7$ GPa. A complete account of this PL phenomenon was reported elsewhere.[21,34]

A salient feature is that the PL properties $I_{PL}(T,P)$ and $\tau(T,P)$ along the series as a function of temperature and pressure can be accounted for on the basis of Eq. (1) by renormalizing the Sr content, x, or the pressure, P, to the lattice parameter, a. Figure 9 displays the calculated $\tau(a)$ curve together with the experimental data obtained along the series at ambient pressure and from pressure spectroscopy.

It is worth noting the adequacy of Eq. (1) to explain the PL properties of the present systems not only in the fluorite phase but also in the cotunnite phase. The calculated $\tau(a)$ curves are referred to a distinct abscissa axis for each phase. The lattice parameter in the cotunnite phase ($Pnma$) (Ref. 18) was derived from the corresponding orthorhombic parameters, a, b, and c, using: $a_{cot} = (abc/2)^{1/3}$ (Refs. 28 and
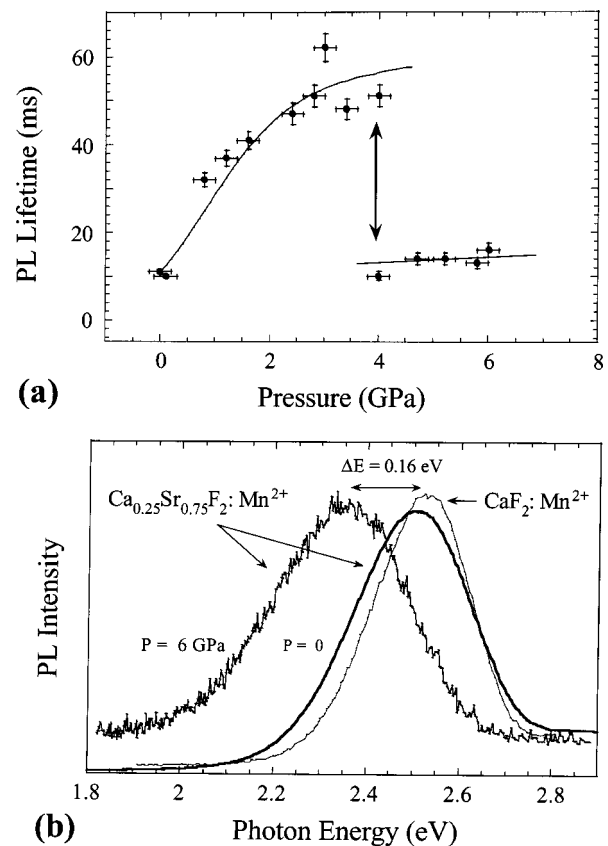

FIG. 8. (a) Variation of the PL lifetime with pressure in Ca$_{0.25}$Sr$_{0.75}$F$_2$: Mn^{2+} at room temperature. The abrupt jump of $\Delta\tau = 40$ ms at $P = 4.0$ GPa corresponds to the fluorite-to-cotunnite phase-transition. The solid line in the fluorite phase corresponds to calculated $\tau(P)$ values from Eq. (1) using parameters $E_a(P)$ and $p(P)$ given in Fig. 5 by renormalizing lattice parameter values to pressure through the Murnaghan's equation of state given in Eq. (3) with $B_0 = 73.4$ GPa and $B' = 5$ (Refs. 22, 28, and 33). Although τ decreases at 4.0 GPa, $I_{PL}(P)$ increases at and above this pressure. (b) PL spectrum of Ca$_{0.25}$Sr$_{0.75}$F$_2$: Mn^{2+} taken above and below the critical pressure, $P = 4.0$ GPa. Note the abrupt redshift of -0.16 eV experienced by the PL band on passing from the fluorite to the cotunnite phase. The PL spectrum of CaF$_2$: Mn^{2+} at ambient conditions is included for comparison purposes.

34). The curves were calculated from Eq. (1) using the same nonradiative rate term, w_{NR}, for both phases but changing the radiative rate: $\tau_0^{-1} = 2.6$ s^{-1} and $\tau_{ED}^{-1} = 3.5 - 0.16 P$ (in s^{-1} and GPa units) for the fluorite phase, and $\tau_0^{-1} = 77.5$ s^{-1} ($\tau_0^{-1} \gg \tau_{ED}^{-1}$) for the cotunnite phase. As we suggested above, the increase of τ_{rad}^{-1} in the cotunnite phase (i.e., reduction of τ_{rad}) is due to odd-parity components of the CF in the ninefold coordination geometry attained at the cation site in the cotunnite phase (Fig. 1). The increase of the ED transition probability thus reduces $\tau(P)$ but increases $I_{PL}(P)$. This model explains why the decrease of $\tau(P)$ observed in Ca$_{0.25}$Sr$_{0.75}$F$_2$: Mn^{2+} above 4 GPa is associated with an increase of $I_{PL}(P)$, in contrast to findings along the series at ambient conditions. In the former case PL changes are related to noncentrosymmetric CF at the cotunnite phase that mainly affects the ED radiative rate. In the latter situation, PL changes are governed by nonradiative processes, which mainly rely on the host crystal volume, but keeping the cubal symmetry at the cation site. Therefore, either an
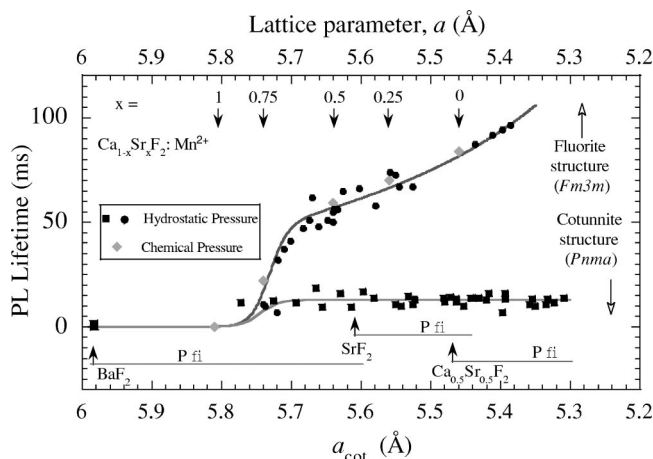
FIG. 9. Variation of the PL lifetime with the lattice parameter, $\tau(a)$, measured as a function of the strontium fraction, x, along the $Ca_{1-x}Sr_xF_2$: Mn^{2+} and BaF_2: Mn^{2+} and from pressure spectroscopy at room temperature in both the fluorite and cotunnite phases. Lifetime data $\tau(a)$ are represented as a function of the lattice parameter for the fluorite and cotunnite phases. In the fluorite phase $\tau(a)$ has been obtained through the linear dependence of a with x for the series (diamonds), and through the corresponding EOS [Eq. (3)] in the hydrostatic pressure experiments (circles). The squares represent the lifetime data in the cotunnite phase. They are referred to the abscissa, a_{cot}, representing the effective lattice parameter in the cotunnite phase, defined as: $a_{cot}=V^{1/3}=(\frac{1}{2}a \cdot b \cdot c)^{1/3}$ where a, b, and c are the orthorhombic lattice parameters. Solid lines have been calculated through Eq. (1) using parameters obtained from intensity and lifetime measurements performed along the series as a function of the temperature

increase or a decrease of $\tau(P)$ is always accompanied by a proportional change of $I_{PL}(P)$, i.e., quantum yield, $\eta(P)$.

Interestingly, these results clearly point out that the PL quenching of Mn^{2+} and the variation of E_a along the series are not directly associated with the different chemical nature of Ca, Sr, and Ba, but related to the crystal volume per molecule. Consequently, $I_{PL}(T,P,x)$ and $\tau(T,P,x)$ are well described as a function of either T or P or x through Eq. (1) by renormalizing pressure data and series results to volume: $I_{PL}(T,V)$ and $\tau(T,V)$. Moreover, the radiationless rate is described by thermal activated processes with pre-pre-exponential factor and activation energy depending only on the crystal volume using the *same parameters* in both phases. This noteworthy result suggests that the nonradiative processes rely on the specific volume irrespective of the local structure around the Mn^{2+} impurity. It turns out that nonradiative multiphonon relaxation can be strongly reduced in the high-pressure phase due to the important volume reduction. This tricky procedure of reducing E_a together with the high phase-transition-hysteresis of these systems can indeed provide new ways for obtaining more efficient PL materials.

IV. CONCLUSIONS AND FINAL REMARKS

We have found a linear variation of the activation energy responsible for the nonradiative process and an exponential behavior of the pre-exponential rate with the specific volume. Thus, nonradiative multiphonon relaxation is enhanced and consequently PL quenched with increasing the host volume. This situation can be reversed by pressure, which modi-

fies E_a and induces a phase-transition to the cotunnite phase with an important volume reduction ($V_{cotunnite}/mol \sim 0.9$ $V_{fluorite}/mol$) (Refs. 28, 34, and 35).

We have shown that PL efficiency along the series as a function of pressure and temperature is mainly related to changes of the nonradiative rate through p and E_a irrespective of the fluorite or cotunnite phase. We describe the associated nonradiative transition rate through an unique expression for all these systems in both phases. The increase of PL, i.e., increase of E_a and decrease of p, is due to the reduction of the cation host size either along the series or in the cotunnite phase in comparison to the fluorite phase. Therefore, the PL decrease by increasing volume is interpreted as the MnF_8^{6-} unit has more space to distort in the excited state, thus leading to a higher Huang–Rhys factor along the series, as it is revealed by the increase of the Stokes Shift on passing from CaF_2 to SrF_2 or BaF_2. The reduction of the electronic transition rate, p, is likely associated with an effective reduction of the electronic interaction responsible for the nonradiative $^4T_{1g} \rightarrow {}^6A_{1g}$ relaxation. The increase of the Jahn–Teller effect in the excited state with increasing volume can probably account for this effect (Ham effect). Work along this line is currently in progress.

According to correlations established between the activation energy, E_a, and the crystal volume, V (and subsequently the lattice parameter, a) along the $Ca_{1-x}Sr_xF_2$: Mn^{2+} series, the structural requirement to induce Mn^{2+} PL in difluorides irrespective of the host crystal structure is a crystal volume smaller than $29 \text{ cm}^3 \text{mol}^{-1}$. Therefore, we could induce PL by applying pressure whatever the lattice parameter decreases below the critical value, $a_{crit}=5.75$ Å.

The pressure-induced phase-transition has revealed the cotunnite phase as an efficient structure for PL to occur. The phase-transition also affects the radiative ED transition rate, τ_{ED}^{-1}, because of the low-symmetry CF at the impurity site. The volume reduction involved in the fluorite-to-cotunnite phase-transition favors PL recovering even in non-PL materials like SrF_2: Mn^{2+} and BaF_2: Mn^{2+}. This phase-transition and particularly the stabilization of the cotunnite phase at ambient conditions can be an attractive way of improving Mn^{2+} PL. The search of materials with large hysteresis offers alternative strategy of this phase at ambient pressure, thus providing new ways for improving PL materials on the basis of high-pressure transformations.

[1] P. A. Alonso and R. Alcalá, J. Lumin. **22**, 321 (1981).
[2] P. Schotanus, P. Dorenbos, C. W. E. Van Eijk, and H. J. Lamfers, Nucl. Instrum. Methods Phys. Res. A **281**, 162 (1989).
[3] R. Visser, P. Dorenbos, C. W. E. van Eijk, and H. W. den Hartog, J. Phys.: Condens. Matter **4**, 8801 (1992).
[4] R. Visser, P. Dorenbos, C. W. E. van Eijk, A. Meijerink, G. Blasse, and H.

W. den Hartog, J. Phys.: Condens. Matter **5**, 1659 (1993).

[5] B. P. Sobolev, E. A. Krivandina, S. E. Derenzo, W. W. Moses and A. C. West, *Scintillator and Phosphor Materials* (Mater. Res. Soc. Symp. Proc. Materials Research Society, Pittsburgh, 1994), Vol. 348, p. 277.

[6] R. J. Richardson, S. Lee, and T. J. Menne, Phys. Rev. B **4**, 1065 (1972).

[7] W. Gehloff and W. Ulrici, Phys. Status Solidi B **102**, 11 (1980).

[8] M. T. Barriuso and M. Moreno, Chem. Phys. Lett. **112**, 165 (1984).

[9] A. G. Badalyan, P. G. Baranov, V. S. Vikhnin, and V. A. Khramtson, Pis'ma Zh. Eksp. Teor. Fiz. **44**, 87 (1986) [JETP Lett. **44**, 110 (1986)].

[10] H. Soethe, V. A. Vetrov, and J. M. Spaeth, J. Phys.: Condens. Matter **4**, 7927 (1992).

[11] M. C. Marco de Lucas, F. Rodríguez, and M. Moreno, J. Phys.: Condens. Matter **5**, 1437 (1993).

[12] S. Sugano, Y. Tanabe, and H. Kamimura, *Multiplets of Transition-Metal Ions* (Academic, New York, 1970).

[13] F. Rodríguez and M. Moreno, J. Chem. Phys. **84**, 692 (1986).

[14] M. C. Marco de Lucas, F. Rodríguez, and M. Moreno, Phys. Rev. B **50**, 2760 (1994).

[15] M. Díaz, F. Lahoz, B. Villacampa, R. Cases, B. Sobolev, and R. Alcalá, J. Lumin. **81**, 53 (1999).

[16] F. Rodríguez, H. Riesen, and H. U. Güdel, J. Lumin. **61**, 581 (1991).

[17] M. C. Marco de Lucas, M. Moreno, F. Rodríguez, and P. G. Baranov, J. Phys.: Condens. Matter **8**, 2457 (1996).

[18] R. W. G. Wycoff, *Crystal Structures* (Wiley, New York, 1963).

[19] F. Rodríguez, I. Hernández, R. E. Gutiérrez, S. García-Revilla, M. Moreno, and R. Alcalá, High Press. Res. **22**, 115 (2002).

[20] I. Hernández, Graduate Thesis, University of Cantabria (2002).

[21] I. Hernández and F. Rodríguez, Phys. Rev. B **67**, 012101 (2003).

[22] R. E. Gutiérrez, F. Rodríguez, M. Moreno, and R. Alcalá, Radiat. Eff. Defects Solids **154**, 287 (2001).

[23] R. Nakata, T. Nakajima, K. Kawano, and M. Sumita, J. Phys. Chem. Solids **52**, 81011 (1991).

[24] A. Jayaraman, Rev. Mod. Phys. **55**, 65 (1983).

[25] S. Koide and M. H. L. Pryce, Philos. Mag. **3**, 607 (1958).

[26] A. B. P. Lever, *Inorganic Electronic Spectroscopy*, 2nd ed., *Studies in Physical and Theoretical Chemistry* (Elsevier, New York, 1984).

[27] B. Henderson and G. F. Imbusch, *Optical Spectroscopy of Inorganic Solids* (Oxford University Press, New York, 1983).

[28] G. A. Kourouklis and E. Anastassakis, Phys. Rev. B **34**, 1233 (1986).

[29] W. B. Holzapfel and N. S. Isaacs, *High-Pressure Techniques in Chemistry and Physics. A Practical Approach* (Oxford University Press, New York, 1997).

[30] J. A. Aramburu, M. T. Barriuso, and M. Moreno, Appl. Magn. Reson. **3**, 283 (1992).

[31] S. Hirako and R. Onaka, J. Phys. Soc. Jpn. **51**, 1255 (1982).

[32] C. K. Jørgensen, *Solid State Physics*, Vol. 13 (Academic, New York, 1962), p. 375; Prog. Inog. Chem. **12**, 109 (1970).

[33] G. Wong and D. E. Schele, J. Phys. Chem. Solids **29**, 1309 (1968).

[34] E. Yu. Tonkov, *High Pressure Phase Transformations. A Handbook* (Gordon & Breach Science Publisher, Amsterdam, 1992), and references given therein.

[35] J. Haines, J. M. Léger, F. Gorelli, D. D. Klug, J. S. Tse, and Q. Li, Phys. Rev. B **64**, 134110 (2001).

[36] G. A. Samara, Phys. Rev. B **2**, 4194 (1970).